Synergism Between Fatigue and Cyclic-Stress Corrosion-Cracking

Meryl M. Hall, Jr.[a*]

[a*]*Independent Researcher, USA*

1366 Hillsdale Dr.

Monroeville, PA 15146

1-412-856-5347

**Corresponding author: hallmm44@comcast.net*

Keywords: aluminum alloy**,** corrosion fatigue, stress corrosion cracking, strain rate, repassivation

HIGHLIGHTS

- Crack tip strain rate (CTSR) is an essential variable for environmental cracking
- CTSR due to fatigue stress-cycles activates additional crack tip surface area
- Increased active surface area increases crack growth rate by an SCC mechanism
- Synergism of fatigue and cyclic-SCC produces rates greater than predicted by superposition
- A model is developed to quantify the effect of fatigue stress-cycles on C-SCC velocity

ABSTRACT

For 50 years, researchers have considered how time-dependent environmental effects can be included in cycle-dependent corrosion fatigue (CF) crack growth rate (CGR) models. Common assumptions are that cycle- and time-dependent contributions are separable, operate in parallel, are non-interacting and that total environmental CGR can be obtained by linear summation of cycle-dependent fatigue and time-dependent (SCC) CGRs. However, considered here are data and analyses that show that environmental CGRs may be greater than predicted by superposition models. A phenomenological model is developed to quantify the effect of crack-tip strain-rate due to fatigue stress-cycles on electrochemical activity at a crack tip and thereby synergistically increase crack growth rates by a cyclic-stress corrosion-cracking (C-SCC) mechanism.

Nomenclature

$\dot{a}$	crack growth rate (CGR)	k^*	time-based passivation rate constant
$\dot{a}^*$	maximum CGR by an environmental mechanism	K	stress intensity factor
$\dot{a}_{\text{inert}}$	Fatigue CGR in an inert environment	$K_{\max}$	maximum stress intensity factor
$\dot{a}_o$	CGR at the start of a hold-time period	M	molecular weight
A^*	electrochemically-active surface area (ECSA) fraction	R-ratio	alternating stress ratio
A_o^*	ECSA at the start of a hold-time period	t_{H}	period of fatigue stress-cycles
A_{sat}^*	Maximum ECSA after a period of fatigue stress-cycles	t_{P}	rise time
A_{scc}^*	Statically-loaded ECSA or after a long hold-time period	t_{R}	hold-time
f	cyclic frequency	γ	strain-based activation rate constant
F	Faraday's constant	$\dot{\varepsilon}$	CTSR due to fatigue stress-cycles
i_a	anodic current density	$\bar{\dot{\varepsilon}}$	CTSR at static load
i_a^*	anodic current density for a fully activated crack tip	ε'	crack tip strain gradient
i_o^*	exchange current density for a fully activated crack tip	θ	proportionality factor

Acronyms

CF	corrosion fatigue	CTSR	crack tip strain rate
CGR	crack growth rate	ECSA	electrochemically-active surface area
C-SCC	cyclic-stress corrosion-cracking	SCC	stress corrosion cracking
CTA	crack tip activity	SET	straining electrode test

1. Introduction

Since the early work of Wei and co-workers Landes (1969)[1] and Gao (1983)[2], researchers have considered how time-dependent environmental effects can be included in existing cycle-dependent fatigue crack-growth-rate (CGR) models. As late as 2017[3], 2018[4], some proposed models continue to assume the "linear superposition" model first proposed by Wei-Landes in 1969. These corrosion fatigue (CF) models assume that cycle- and time-dependent contributions are separable, operate in parallel and are non-interacting. Wei

(2002)[5] summarizes a later version of his superposition model, which includes four "mechanistic" components that operate independently within surface-areas associated with each. Several superposition models, mostly variations on Wei-Landes, have been developed and applied to specific alloys and environments, with varying degrees of success[6, 7, 8].

The time-dependent component of superposition models is simply calculated using stress corrosion cracking (SCC) correlations[5]. This approach assumes implicitly that static-stress SCC crack-growth-rate (CGR) mechanism is a unique function of the instantaneous stress intensity factor, unaffected by time-dependent variation of K. However, there are many examples that show that SCC CGR is not a unique function of K[9,10] but is dependent on the kinematics of loading.

Other researchers[11,12] have explored experimentally the potential synergistic interactions between fatigue and SCC mechanisms. Respectively, they tested a 2024 aluminum alloy at room temperature in a 3.5% NaCl aqueous solution and Alloy 600 in high temperature water at 290°C with 4 ppm dissolved oxygen. They conducted inert environment fatigue tests, statically-loaded SCC tests and environmental fatigue tests where both fatigue and SCC mechanisms are present. Both researchers found that crack growth rates in environmental fatigue tests are larger than that predicted by superposition models. They found that the increase in CGR is controlled by the load rise-time of the upload half-cycle and speculated that the resultant CGR is due to a synergistic interaction of fatigue and SCC mechanisms of crack advance.

The purpose of this study is to consider how cycle-dependent fatigue and time-dependent SCC mechanisms can act synergistically to produce environmental crack growth rates greater than predicted by simple superposition models. A phenomenological model is developed to quantify the effect of crack tip strain rate (CTSR), following a fatigue stress-cycle, on cyclic-stress corrosion-cracking (C-SCC) crack growth rate. This C-SCC model is calibrated using hold-time CGR data obtained on high strength aluminum alloy 7278-T6 and tested in a 3.5% NaCl aqueous solution.

2. Theory

2.1 Phenomenological models

The inherent complexity of corrosion fatigue gives rise to complex mechanistic models with a large number of variables and parameters. Details of these models have been exhaustibly covered in the literature[3,4,13, 14, 15] and the additional references found in these papers. These references illustrate that corrosion fatigue is a complex function of multiple materials and environmental variables.

However, the behavior of several mechanisms operating collectively often can be characterized by a relatively smaller number of phenomenological variables and parameters that are motivated by mechanistic considerations. Phenomenological models involve a continuum level of detail and avoids modeling of discrete elements at the microstructural and higher-levels of details.

A phenomenological model describes the empirical relationship of phenomena one to another, consistent with assumptions of the underlying mechanisms. Variables and parameters of phenomenological models have physical meanings that enhance the interpretability of the model.

Not considered here are the scientific details of the chemical and electrochemical processes that contribute to anodic and cathodic current densities at a crack tip[3,4,13-15]. Phenomenological assumptions regarding electrochemical activity of crack tips are discussed in the literature[4,16] and many other references that can be found by a literature search.

CTSR is considered to be an essential mechanical variable contributing to SCC CGR[17]. However, CTSR has been treated incorrectly in model development[17] and expressions for CTSR have been incorrectly derived[18]. The model developed here assumes that components of CTSR, and rate constants for crack tip activation and repassivation, determine the magnitude of the electrochemically-active surface area (ECSA)-fraction at a crack tip. A phenomenological model is developed to quantify the effect of crack tip ECSA-fraction on environmental crack growth rate.

2.2 Components of environmental crack growth rate

Considered here is that the total environmental crack growth rate, $\dot{a}_{env}$, consists of two components, cycle-dependent "true corrosion fatigue" (TCF), $\dot{a}_{tcf}$, and time-dependent "cyclic-stress corrosion-cracking" (C-SCC), $\dot{a}_{c\text{-}scc}$. The TCF component is environment-assisted but is cycle-dependent, only. TCF has been modeled successfully[19] as proportional to inert environment fatigue $\dot{a}_{tcf} = \theta(K)\,\dot{a}_{inert}$. The $\left(\frac{da}{dN}\right)_{TCF} = \Theta\left(\frac{da}{dN}\right)_{inert}$ proportionality factor was found to be as large as 10 x at low stress intensity factor, K, and decreases to 1 x as K increases. When there is no environmental effect on the cycle-dependent component, $\dot{a}_{tcf} = \dot{a}_{inert}$.

The C-SCC component[20, 21, 22, 23, 24] is environment-driven, is time-dependent but is accelerated by fatigue stress-cycles. C-SCC is determined experimentally as the difference between $\dot{a}_{env}$ and $\dot{a}_{tcf}$. Then TCF represents environmental enhancement of a cycle-dependent mechanical crack advance mechanism and C-SCC represents mechanical enhancement of a time-dependent environmental crack advance mechanism.

Cyclic-stress corrosion-cracking is so named to emphasize that fatigue stress-cycles can increase the activity of time-dependent SCC crack growth mechanisms. When there are no fatigue stress-cycles, C-SCC = SCC. As fatigue stress-cycles increase in frequency, the cycle-dependent TCF mechanism increasingly overcomes the time-dependent C-SCC mechanism.

2.3.1 Crack tip activity

A single crack advance mechanism by film-rupture – active-path dissolution (FR/APD)[25,26] is assumed here in order to simplify the equation development. Note that FR of a protective crack-tip film also enables hydrogen-uptake and crack advance by a hydrogen environment cracking mechanism[27] (FR/HE).

When cracks advance by the FR/APD mechanism[28] the crack growth rate is given by Faraday's Law of Electrolysis,

$$\dot{a} = \frac{M}{z\rho F} i_a \quad , \qquad 11\text{* MERGEFORMAT ()}$$

where $\dot{a}$ is quasi-steady-state CGR (da/dt), M is molecular weight, z is charge of the metal cation, ρ is density, F is Faraday's constant. The anodic current density, i_a, is a measure of electrochemical activity at a crack tip. This equation says that to increase $\dot{a}$, one needs to increase the anodic current density. This can be done by increasing the electrochemically-active surface area (ECSA)-fraction, A^* [29]:

$$i_a = i_a^* A^* \quad , \qquad 22\text{* MERGEFORMAT ()}$$

where i_a^* is the current density measured on a fully activated surface.

2.2 Electrochemically-active surface area model

ECSA[30, 31] of a crack tip is an important property as it is a function of a prime essential variable, CTSR. Customary assumptions of FR/APD stress corrosion modeling[5] are that (1) crack tip activity (CTA) is determined by the competitive rates of crack tip activation and repassivation, (2) when the crack tip environment favors passivation, dynamic CTSR is required to activate crack tips by rupturing protective oxides and generating electrochemically-reactive emergent-dislocations and slip lines, (3) the surface simultaneously may passivate by dissolution of newly exposed active metallic surfaces and by reformation of protective surface films. In order to simplify model development, fractions of the surface are treated as either active having active surface-fraction A^*, or inactive having surface area-fraction $1 - A^*$.

The instantaneous magnitude of A^* depends on the relative rates of strain-rate-driven crack tip activation and time-dependent passivation. The time-based rate of change of A^* is given by

$$\frac{dA^*}{dt} = -k^* A^* + \gamma \dot{\varepsilon} (1 - A^*) \quad , \qquad 33\text{* MERGEFORMAT ()}$$

where the first term on the right-hand side is the rate with which an active surface is passivated, the second term is the rate with which passivated surface is activated. In this equation, $\dot{\varepsilon}$ is the total strain rate from all contributions, k^* is the time-based surface passivation rate constant, and γ is the strain-based surface activation rate constant. When all crack tip strain contributes to surface activation, $\gamma \equiv 1$.

For an initially passive surface, $A^* = 0$ and $dA^*/dt = \gamma\dot{\varepsilon}$ so that CTA is rate-limited by the applied strain rate. For a fully active surface, $A^* = 1$ and $dA^*/dt = -k^*$ so that CTA is rate limited by the passivation rate. For cases that lie between these limits, passivation rate and CTSR rate are competitive rate-determining processes.

2.3 Crack tip strain rate

Inelastic CTSR is considered here to include three components; strain rate due to variations in applied load, $\dot{\tilde{\varepsilon}}$, time-dependent strain rate, $\dot{\bar{\varepsilon}}$ (high-stress low-temperature creep[32]) and strain rate due to advance of a crack into the negative elastic-plastic strain gradient lying ahead of the advancing crack, $\dot{\varepsilon}'$. The first component is a function of $\dot{K}$, the second and third are functions of $\dot{a}$. For steady-state "creep-brittle" crack growth[33] – where an embrittled fracture process zone (FPZ) is embedded in an otherwise ductile metal – the rate of stress elevation due to crack advance is just balanced by the rate of stress relaxation. This is consistent with an assumption that creep-brittle cracks grow at a rate that maintains pace with growth of the FPZ.

For expediency and clarity of expression, CTSR is represented symbolically as $\dot{\varepsilon} = \dot{\tilde{\varepsilon}} + \dot{\bar{\varepsilon}} + \dot{\varepsilon}'$ (explicit expressions can be found in the literature[34,35.]). Strain rate due to crack advance can be expressed as $\dot{\varepsilon}' = |\varepsilon'|\dot{a} = |\varepsilon'|\dot{a}^* A^* \equiv \dot{\varepsilon}^* A^*$ where $\varepsilon' \equiv \left(\partial\varepsilon/\partial r\right)_t$ is the crack tip strain gradient and $\dot{a}^*$ is a reference crack velocity associated with a fully activated crack tip ($A^* = 1$). Incorporating these strain rate components, Eq. 3 can be written as

$$\frac{dA^*}{dt} = -kA^* + \gamma\left(\dot{\tilde{\varepsilon}} + \dot{\bar{\varepsilon}}\right) - \gamma\dot{\varepsilon}^* A^{*2} \quad , \quad 44\text{* MERGEFORMAT ()}$$

where $k \equiv k^* + \gamma(\dot{\tilde{\varepsilon}} + \dot{\overline{\varepsilon}} - \dot{\varepsilon}^*)$. Using equation 2, Eq. 1 can be written as

$$\dot{a} = \frac{Mi_a^*}{z\rho F} A^* \equiv \dot{a}^* A^* \quad , \qquad 55\text{* MERGEFORMAT ()}$$

where $\dot{a}^*$ is the maximum crack growth rate attainable by a time-dependent mechanism. For crack velocities greater than $\dot{a}^*$, the C-SCC crack advance mechanism is overdriven by either TCF or a purely mechanical mechanism.

Useful physical interpretations of Eqs. 2 and 5 are that A^* is a normalized current density, $A^*(t) = i_a(t)/i_a^*$, and a normalized crack growth rate, $A^*(t) = \dot{a}(t)/\dot{a}^*$. Then an analysis to determine A^* is an analysis to determine both these normalized variables.

2.4 Limiting solutions for A^*

2.4.1 Cyclic loading without hold-time

Integration of Eq. 4 results in a complex set of equations[36] that are difficult to simplify except in some limiting cases that are useful for ease of analysis and understanding the significance of active surface area and CTA. Recalling that creep and crack advance strain rates are functions of $\dot{a}$, the CGR data analyzed in Section 4 shows that the CTSR component $\dot{\tilde{\varepsilon}}$, due to rapid load cycling without hold-time, can be two orders of magnitude larger than that due to creep $\dot{\overline{\varepsilon}}$ and crack advance $\dot{\varepsilon}'$. In this case, the CTSR components due to creep and crack advance can be ignored. On integration, Eq. 4 becomes

$$A^* = A_o^* \mathrm{e}^{-kt} + \frac{\gamma\dot{\tilde{\varepsilon}}/k^*}{1+\gamma\dot{\tilde{\varepsilon}}/k^*}\left(1-\mathrm{e}^{-kt}\right) \quad , \qquad 66\text{* MERGEFORMAT ()}$$

where $k \equiv k^*\left(1+\gamma\dot{\tilde{\varepsilon}}/k^*\right)$. It is assumed that activation of the crack tip occurs mainly during the up-load half cycle[4,37] which is implemented by letting $\gamma = 1$ during the up-load half-cycle and $\gamma = 0$ during the down-load half-cycle.

Eq. 6 shows that A^* increases during up-loading and decreases exponentially during down-loading. On up-loading A^* approaches a maximum value of

$$A^*_{sat} = \frac{\gamma\dot{\varepsilon}/k^*}{1+\gamma\dot{\varepsilon}/k^*}. \qquad (77)$$

Saturation value of A^* typically can be attained after only a few continuous load cycles. Note that $A^*_{sat} \to 1$ only if $\gamma\dot{\varepsilon} \gg k^*$, that is, only if the crack tip activation rate far exceeds the passivation rate, as may occur during rapid fatigue load cycling and when crack tip chemistry does not favor passivation.

2.4.2 Hold-time following a stress cycle

Another case of interest is crack growth during a hold-time $\left(\dot{\varepsilon}=0\right)$ at $K = K_{max}$ following a period of fatigue cycles. The data analyzed here show that at the moment that stress cycling is stopped at K_{max}, the crack velocity (da/dt) remains comparable to the fatigue crack velocity but then decreases according to second-order kinetics to the statically-loaded SCC crack velocity. Then, assuming $\dot{\varepsilon}=0$, initially $\dot{\varepsilon}^* \gg \dot{\varepsilon}$ and second order passivation rate kinetics, the ECSA-fraction rate equation, after rearranging terms, becomes

$$\frac{dA^*}{dt} = -kA^{*2} + \gamma\dot{\varepsilon}^* A^*, \qquad (88)$$

where $k \equiv k^*\left(1+\gamma\dot{\varepsilon}^*/k^*\right)$. This equation can be integrated to find

$$A^* = \frac{\left(\gamma\dot{\varepsilon}^*/k\right)A^*_o}{\left(\gamma\dot{\varepsilon}^*/k\right)e^{-\frac{\gamma\dot{\varepsilon}^*}{k}kt} + A^*_o\left(1-e^{-\frac{\gamma\dot{\varepsilon}^*}{k}kt}\right)}, \qquad (99)$$

Eq. 9 has the limits $A^*\left(t=0\right) = A^*_o$ where A^*_o is taken to be the ECSA-fraction at the moment that the up-load half-cycle ends, that is, when the hold-time period begins and which time the

crack velocity is $\dot{a}_o$. For long hold-times, A^* approaches a time-independent value, which is the active surface area-fraction of a statically-loaded stress corrosion crack.

$$A^*_{\text{scc}} = \frac{\gamma\dot{\varepsilon}^*}{k} = \frac{\gamma\dot{\varepsilon}^*/k^*}{1+\gamma\dot{\varepsilon}^*/k^*} = \frac{\gamma|\varepsilon'|\dot{a}^*/k^*}{1+\gamma|\varepsilon'|\dot{a}^*/k^*} \quad .1010\text{* MERGEFORMAT ()}$$

2.5 Application

2.5.1 Straining electrode tests

A great deal of information relevant to the time-dependence of corrosion fatigue data can be obtained from a straining electrode test (SET). The SET is a uniaxial tensile test subject to constant strain rate in a corrosive environment for which corrosion current is measured and electrode voltage is either measured or applied. Recalling that $i_a(t)/i_a^* = A^*(t)$, Eq. 2, Eq.6 can be used to calculate i_a during the up-load cycle and Eq. 7 can be used to calculate $i_{a,sat}$. Eq. 9 can be used to calculate i_a during the down-load cycle.

An example of the effects of dynamic strain rate on current density is the straining electrode results obtained by Huang et al[38]. They tested commercially pure iron in an aqueous solution of 0.2 m/l NaOH polarized potentiostatically at 150 mV vs. HgO/Hg/0.2 M NaOH. Figure 1 shows the anodic current density measured during up-loading at a constant strain rate of 1.1 x 10^{-5}/s, which is followed by a period during which load is held static at 260 MPa (0.09 plastic strain).

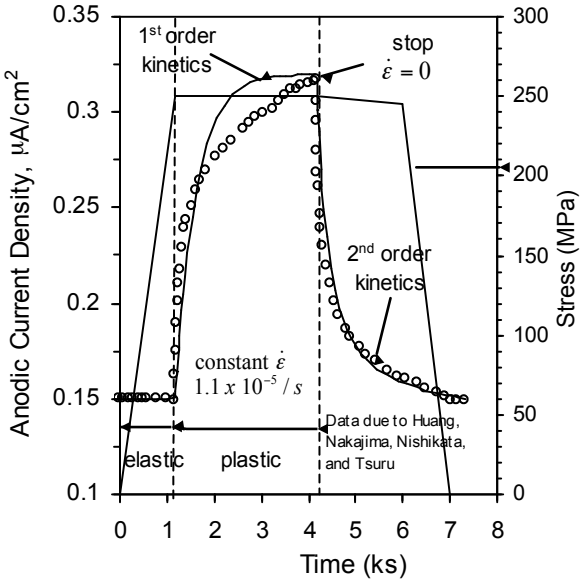

228

229 Fig. 1. Effect of elastic and plastic strain rates on anodic dissolution current density. Straining
230 electrode tests of pure iron in an aqueous solution of 0.2 m/l NaOH polarized potentiostatically at 150
231 mV vs. HgO/Hg/0.2 M NaOH. No effect of elastic-loading but strong plastic effect on current density
232 shows that plastic straining is necessary to electrochemically activate the test electrode.

233

234 The specimen was pre-stressed to a stress level of 260 MPa then passivated stress-
235 free for a 24-hour period, during which a stable passive current of about 0.15 μA/cm^2 was
236 established. Following pre-stress, stress increases at first elastically up to the last yield point
237 of 260 MPa. During elastic loading there is no increase in the anodic current above the static
238 passivation current level, showing that plastic strain is required to activate the specimen
239 surface. On yielding, the current increases very rapidly and appears to be approaching
240 saturation. When plastic straining is stopped, the current trend is reversed and current
241 decays back to the original passive current level. Only the current density in excess of the
242 passivated electrode current-density was considered in analyzing the data.

243 Recall again that the normalized anodic current density (ACD) is directly proportional
244 to A^*, the up-loading curve marked "1st order kinetics" represents the best fit of the up-
245 loading ACD data using Eq.6, which was derived assuming first-order passivation rate
246 kinetics, $\left(\partial A^*/\partial t\right)_\varepsilon = -k^* A^*$. The repassivation rate curve marked "2nd order rate kinetics",

247 provides a good fit to the hold-time data using Eq. 9, which was derived assuming second-
248 order rate kinetics, $\left(\partial A^*/\partial t\right)_e = -k^* A^{*2}$.

249 This may indicate that at the slower strain rate of the Huang et al. test, both 1st and 2nd
250 order reactions are involved as activation and passivation processes become more
251 competitive. One possibility that could account for second-order rate kinetics during current
252 decay is that the current density reaction rate is limited by a second-order cathodic reaction
253 such as slow-recombination of two adsorbed hydrogens to form molecular aqueous
254 hydrogen[39], that is, $2H_{ads} + M \xrightarrow{rds} H_2(a) + M$.

255 Note that passivation following a period of dynamic straining in a straining electrode
256 test, Fig. (1), occurs on the order of kilo seconds. Compare this with results of the usual
257 testing to obtain passivation rate constants k^* for input to aqueous corrosion cracking
258 models[40, 41]. These tests are usually conducted on strain-rate free electrodes that are either
259 electrically or mechanically "cleaned" of oxide to expose fresh metal surfaces. Results of
260 these strain-free static tests show that repassivation occurs on the order of milliseconds.
261 This comparison shows that plastic strain activates surfaces well beyond that of a strain-free
262 bare metal surface.

263 **3. Material and methods**

264 Time-domain CGR data (da/dt) found in the corrosion fatigue literature are replotted
265 here so-as-to illustrate application of the theory developed above. Of the limited number of
266 papers found in the literature[20-24] on the subject of C-SCC, the corrosion fatigue experiments
267 found in the papers published by Shiozawa[21,22] are analyzed here. Detailed discussions (in
268 Japanese) of test methods are provided in these papers. Briefly, the Shiozawa fatigue tests
269 were conducted in 3.0% NaCl aqueous solution at 15 °C using single-edge-notched
270 specimens (tensile axis aligned with rolling direction) of high strength aluminum alloy 7278-
271 T6.

272 Three types of tests were conducted by Shiozawa. All tests were conducted under
273 load control, R = 0. Continuous-cycling CF tests without hold-time were conducted using
274 triangular wave form with rise times of 22.5 s and 55 s. Continuous-cycling tests (N-cycles)
275 with hold-time were conducted using trapezoidal wave form and rise times as in the cycling

without hold-time tests. Statically-loaded SCC tests without prior load cycles also were conducted over the range of K values corresponding to the range of K_{max} values used in the hold-time tests. Hold-time tests were conducted as illustrated in Fig. 2.

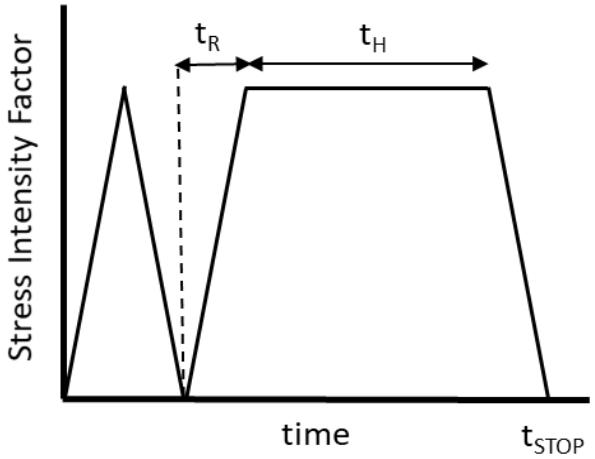

Fig. 2. Schematic representation of the stress cycle used to obtain hold-time data. Following one cycle without hold-time, hold-time tests were conducted with load increased and held constant at K_{max}. Tests were conducted using two load rise times, 22.5 s and 55 s.

Following one cycle without hold-time (N = 1) and by reloading to K_{max}, hold-time tests were conducted with load held constant at K_{max}. For the tests with a rise time of 55 s, hold-times were for 180 s, 600 s and 2700 s. For the tests with a rise time of 22.5 s, hold-times were for 6 s, 12 s, 60 s, 360 s and 3600 s. Crack size was measured at intervals, using a measuring microscope, without interrupting the experiment.

The CGR data are reported as both $\Delta a/\Delta N$ and $\Delta a/\Delta t$ where the latter is determined as $\Delta a/\Delta t = \left(\Delta a/\Delta N\right)/t_p$ and $t_p = 2t_R + t_H$ is the cyclic period. Then, in order to compare predictions of the instantaneous ECSA-fraction equations to the data, Eqs. 6 and 9 must be

integrated over the cyclic period. This is done numerically using the trapezoidal rule[42] repeated and summed over n discrete intervals.

4. Results

The goal of the analysis is to quantify the hold-time behavior of Shiozawa's data using model Eqs. 9 and 10. The first step is to obtain a value for $\dot{a}^*$, which is the maximum crack growth rate attainable by a time-dependent environmental mechanism. This can be estimated using Fig. 3(a) and 3(b) which, respectively, show the 55 s and 22.5 s rise time data (*da/dN*) plotted versus K_{max}.

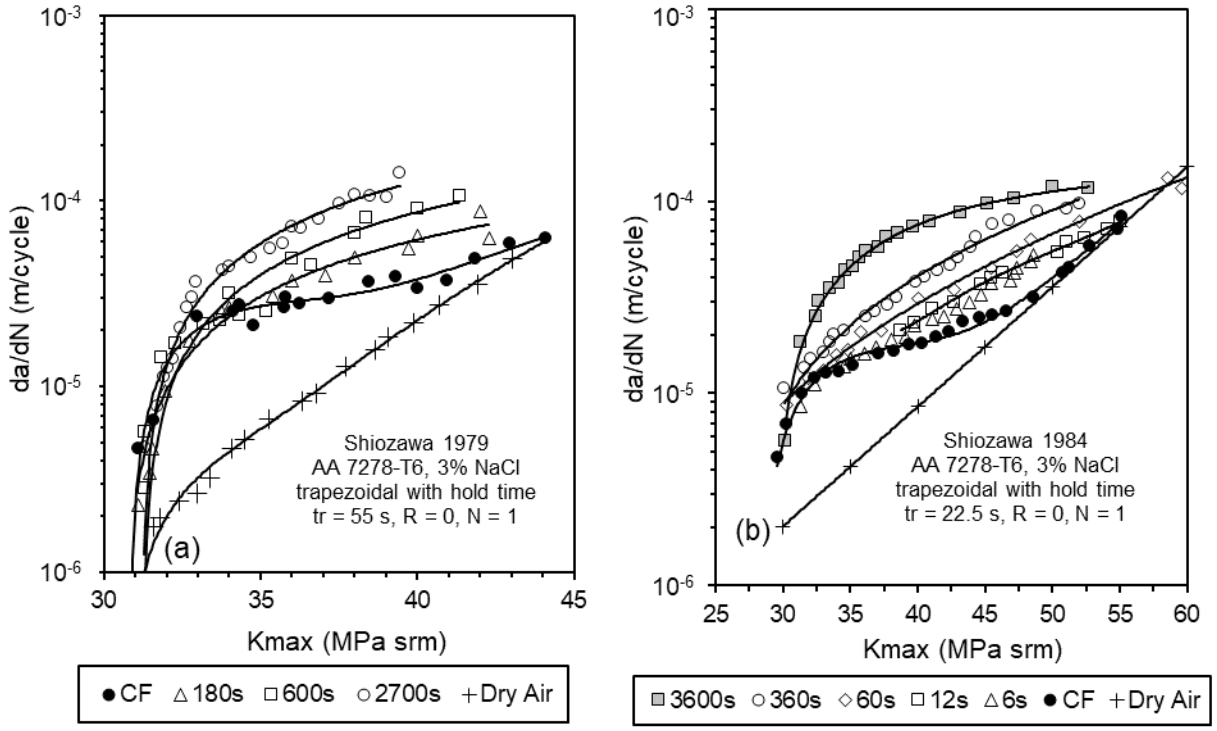

Fig. 3. Crack growth rate (*da/dN*) as a function of K_{max} for a range of hold-times: 3(a) rise time = 55 s, 3(b) rise time = 22.5 s. Convergence of the dry air and CF (w/o hold) data at the upper end of the K_{max} range establishes an upper limit for the occurrence of time-dependent crack growth mechanisms. For crack velocities greater than this, crack growth is rate limited by either true fatigue corrosion or purely mechanical mechanisms.

Fig. 3(a) and 3(b) show that the CF (no hold-time) and dry air crack growth rates (*da/dN*) converge at about 7 x 10^{-5} m/cycle (t_R = 55 s) and 3 x 10^{-5} m/cycle (t_R = 22.5 s) which

implies that $\dot{a}^*$ has a value of about 6.4 x 10^{-7} m/s and 6.7 x 10^{-7} m/s, respectively. This result shows that $\dot{a}^*$ is independent of frequency. An average value of 6.55 x 10^{-7} m/s is applied to the data analyses.

As shown most clearly in Fig. 3(b) for CGR greater than $\dot{a}^*$, CGR is equal to the dry-air CGR, which implies that CGR is limited by environment unaffected, cycle-dependent mechanical mechanisms. Crack velocities less than $\dot{a}^*$ show that time-dependent mechanisms are operable down to an apparent threshold of about 30 MPa√m.

Figures 4 (a) and 4(b) show the *da/dN* data of Fig. 3(a) and 3(b) plotted as crack velocity (*da/dt*) versus K_{max}.

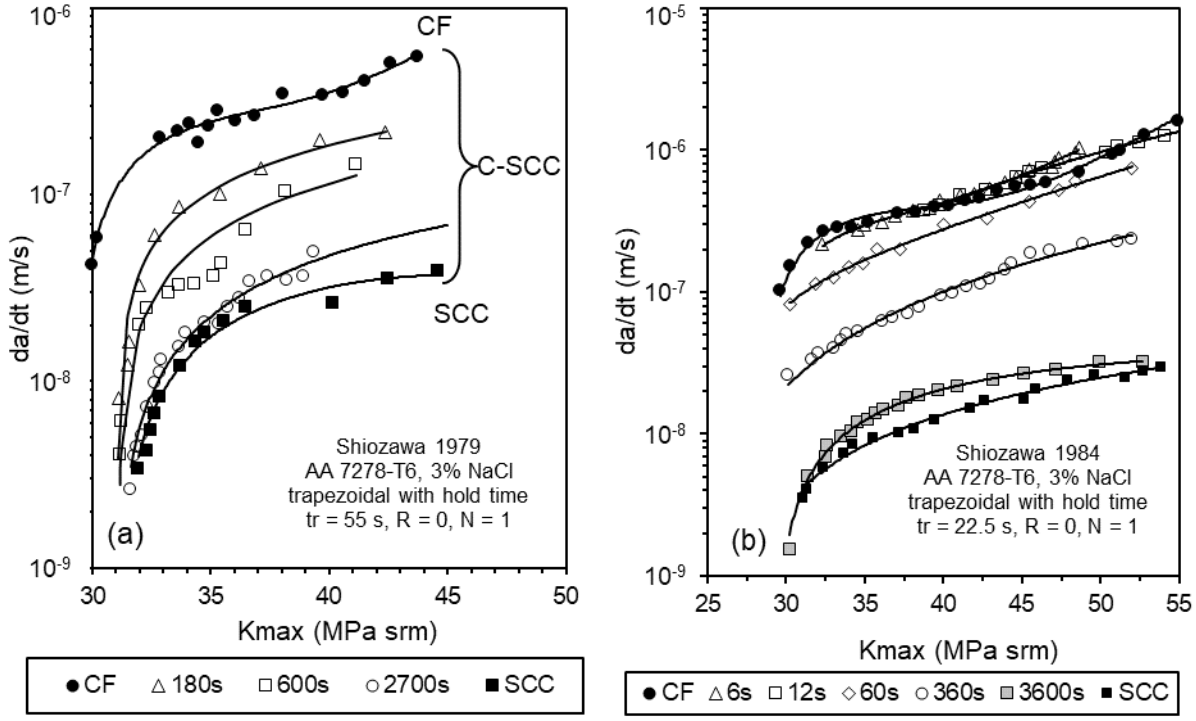

Fig. 4. Crack velocity (da/dt) plotted versus K_{max} for a range of hold-times: 4(a) rise time = 55 s, 4(b) rise time = 22.5 s. The data suggest that there is a continuous trend in crack velocity that links corrosion fatigue (w/o hold-time) and static-stress corrosion-cracking (unlimited hold-time).

These figures show that CF (no hold-time) crack velocity exceeds statically-loaded SCC crack velocity by an order of magnitude or more. Fig. 4(b) shows that crack velocities after 6

s and 12 s hold-times are comparable to the CF rate. Following a load cycle, crack velocity decreases with increasing hold-time and approaches that of statically-loaded SCC for hold-times greater than 2700 s, Fig. 4(a), or 3600 s, Fig. 4(b).

These data trends show that statically-loaded CGR during hold-times following a load-cycle is not a unique function of the applied K but depends on the kinematics of the prior loading and hold-time. The data suggest that there is a continuous trend in crack velocity that links continuous-cycle corrosion-fatigue and SCC. The apparent effect of a load cycle on hold-time CGR at K_{max} is an illustration of C-SCC.

The next step is to determine $A^*_{scc} = \dot{a}_{scc}/\dot{a}^*$ $A^*_{scc} = \frac{\dot{a}_{scc}}{\dot{a}^*}$ using measured values of $\dot{a}_{scc}$ and $\dot{a}^*$ $\dot{a}_{scc}$. Then, using Eq. 10, values are found for the ratios $\gamma\dot{\varepsilon}^*/k$ and $\gamma\dot{\varepsilon}^*/k^*$. A value for $A^*_o = \dot{a}_o/\dot{a}^*$ can be determined using measured values for $\dot{a}_o$, which is the CGR at the beginning of the hold-time.

With these parameters determined, Eq. 9 can be used to obtain a value for k by adjusting k to fit the hold-time data as shown in Fig. 5(a) and 5(b).

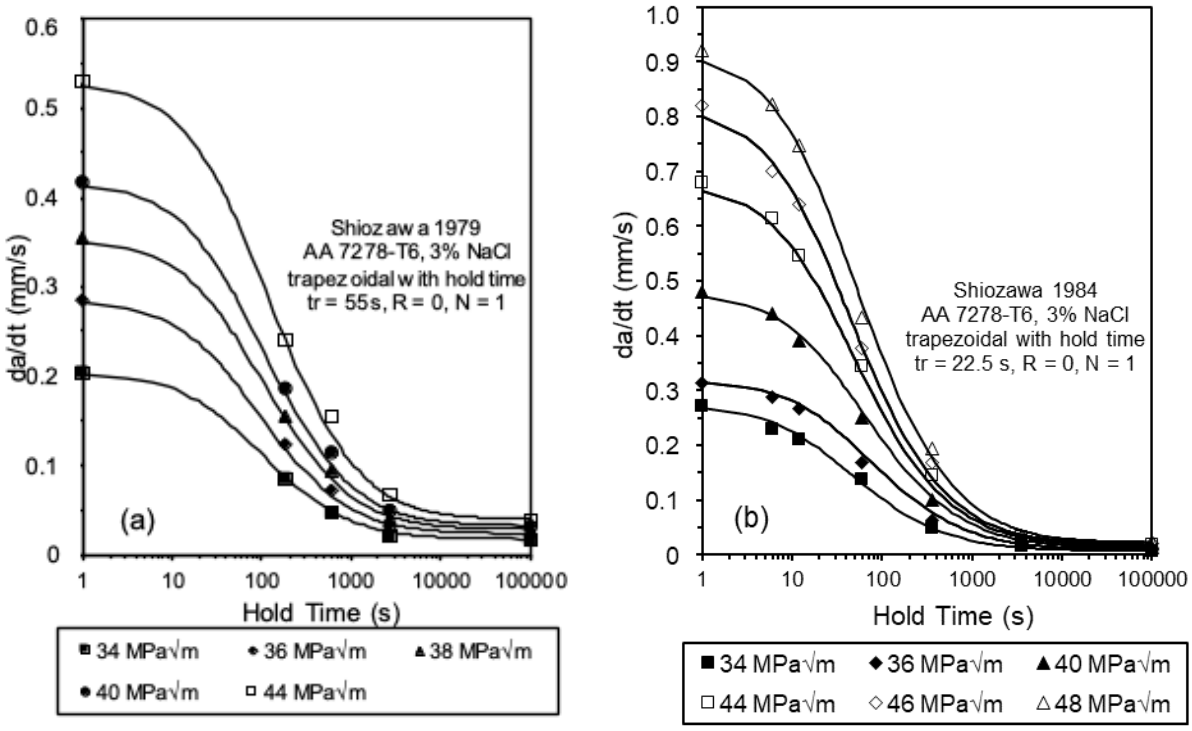

Fig. 5. Crack velocity da/dt plotted versus hold-time for a range of K_{max}: 5(a) rise-time = 55 s, 5(b) rise-time = 22.5 s. Data trend lines are drawn using model Eq. 9 and adjusting the value of k to get the best fit to the data.

These figures show a cross-plot of Fig. 4(a) and 4(b) data plotted as CGR (da/dt) versus hold-time for a range of applied K_{max}. In order to display all the data on one log-scale, the CF without hold-time data are plotted at 1 s and the statically-loaded SCC data are plotted at 100,000 s.

These figures show that crack velocity during continuous load cycling is an order of magnitude larger than the statically-loaded SCC crack velocity. Increasing the up-loading rate by a factor of 2.4 results in a comparable increase in the C-SCC acceleration factor. Moreover, it takes in excess of 2700 to 3600 s of hold-time to approach the SCC crack velocity. This relaxation time is comparable to that of the straining electrode tests of Huang et al and is orders of magnitude greater than the time (< 1 s) to repassivate a static electrode in a chemistry that is representative of a propagating crack. This result emphasizes the importance of the CTSR due to crack advance in delaying passivation.

5. Discussion

5.1 Cyclic-stress corrosion-cracking

Shiozawa makes no claim that FR/APD is the crack advance mechanism and provided no discussion regarding microstructural crack path, either intergranular or transgranular. However, previous studies of high strength aluminum alloys show that transitions in fracture modes, from brittle intergranular to brittle transgranular and more ductile transgranular, occur as the independent variables frequency and ΔK (and dependent variable CGR) are increased above critical levels[43,44].

The data trend lines in Figs. 3(a) and 3(b), show that the cracking mechanism is unaffected by environment for K_{max} greater than about 44 MPa√m to 47 MPa√m where corrosion fatigue (without hold-time) and the dry air data trends converge (typically ductile transgranular cracking mode). For K_{max} less than this, the time-dependence of the data show that the cracking mechanism is environmentally affected.

The data trends in Figs. 4(a) and (b) suggest that, below critical values of K_{max}, continuous-cycle CF and statically-loaded SCC mechanisms act synergistically to accelerate environmental crack growth, C-SCC. Others[45] also have interpreted similar data as showing a synergistic interaction of corrosion fatigue and stress corrosion cracking.

5.2 Model parameters

Model parameters are found in Tables I and II. The information found in these tables show that, when K_{max} increases from 34 MPa√m to 48 MPa√m, the electrochemically-active surface area for statically-loaded SCC, A^*_{scc}, increases from about 1% to 5%. We speculate that these low numbers are due to the electrochemically-active surface being concentrated at grain boundaries. Heat treatable high strength aluminum alloys are susceptible to intergranular corrosion (IGC) and SCC due to selective attack of grain boundary (GB) precipitates and precipitate free zones (PFZ) formed adjacent to grain boundaries during heat treatment.

Maa et al[46] studied formation of PFZs adjacent to grain boundaries in high-strength AA7075, similar in alloy concentrations to AA7278, and found that for a sub-grain/grain size

of about 6 μm the ratio between the width of a PFZ and the grain size (GB spacing) is about 5 % and smaller for larger grains. Harrison et al.[47] reported more detailed measurements of grain size on AA7075-T651 plate and found, with 95% confidence, surface grain sizes of 4.6 μm to 12.1 μm in width, 7.1 μm to 18.9 μm in length and 1.5 μm to 4.0 μm in thickness. For cracks that grow in the thickness direction (T-S or L-S), these numbers support the notion that electrochemically-active surface area is concentrated at grain boundaries during intergranular SCC crack growth.

For continuous cycling A_o^* increases from 22 % to 100 % as K_{max} increases from 34 MPa√m to 48 MPa√m. As discussed in section 5.1, the data show that the cracking mechanism is time-dependent for K_{max} less than about 44 MPa√m to 47 MPa√m. For K_{max} greater than this, the cracking mechanism is unaffected by environment as continuous cycling corrosion fatigue and the dry air data trends converge (typically ductile transgranular cracking mode). This establishes an upper limit for the occurrence of time-dependent crack growth mechanisms. For crack velocities greater than this, time-dependent crack growth is rate limited by either cycle-dependent TCF or purely mechanical mechanisms. We conjecture that continuous cycling significantly increases the electrochemically-active surface area, from intergranular to transgranular, accounting for the increase in A_o^* from 22 % to 100 % and that the increase is due to the C-SCC crack advance mechanism being overdriven by competitive mechanical fatigue mechanisms.

Note that the ratio of activation due to crack advance and repassivation rate constants, $\gamma\dot{\varepsilon}^*/k^*$, is about 1 % to 5 %, consistent with Eq. 10 for A_{scc}^*. This means that the strain-based activation rate constant is only 1 % to 5 % of the repassivation rate constant for statically-loaded SCC.

Table I. Model parameters for hold-time data (rise time 55 s)

Parameter	Value					
K_{max} (MPa√m)	34	36	38	40	44	48
$\dot{a}_{scc}\ (m/s)$	1.61E-08	2.24E-08	2.73E-08	3.14E-08	3.83E-08	4.41E-08
A_{scc}^*	0.0170	0.0237	0.0289	0.0332	0.0406	0.0467

$\dot{a}^*(m/s)$	6.55E-07	6.55E-07	6.55E-07	6.55E-07	6.55E-07	6.55E-07
$\gamma\dot{\varepsilon}^*/k^*$	0.0173	0.0243	0.0297	0.0344	0.0423	0.0490
$\dot{a}_o(m/s)$	2.04E-07	2.85E-07	3.54E-07	4.17E-07	5.30E-07	6.31E-07
A_o^*	0.216	0.302	0.375	0.442	0.561	0.668
$k^*(1/s)$	0.1050	0.0800	0.0600	0.0500	0.0350	0.0150
$\gamma\dot{\varepsilon}^*(1/s)$	0.0018	0.0019	0.0017	0.0017	0.0014	0.0007

Table II. Model parameters for hold-time data (rise time 22.5 s)

Parameter	Value					
K_{max} (MPa√m)	34	36	38	40	44	48
$\dot{a}_{scc}(m/s)$	7.58E-09	9.72E-09	2.73E-08	1.36E-08	1.77E-08	2.24E-08
A_{scc}^*	0.0132	0.0171	0.0289	0.0240	0.0310	0.0390
$\dot{a}^*(m/s)$	6.55E-07	6.55E-07	6.55E-07	6.55E-07	6.55E-07	6.55E-07
$\gamma\dot{\varepsilon}^*/k^*$	0.0134	0.0173	0.0297	0.0244	0.0320	0.0408
$\dot{a}_o(m/s)$	2.75E-07	3.20E-07	3.54E-07	4.80E-07	6.80E-07	9.20E-07
A_o^*	0.481	0.559	0.375	0.839	0.950	----
$k^*(1/s)$	0.080	0.080	0.060	0.055	0.040	0.025
$\gamma\dot{\varepsilon}^*(1/s)$	0.00106	0.00136	0.00173	0.00131	0.00124	0.00098

411 **5.3 Cycle-Domain Superposition Models**

412 According to the Wei-Landes superposition model[5], the behaviors illustrated in Figs.
413 3(a) and 3(b) can be modeled as a simple superposition of cycle- and time-dependent
414 components where the latter is calculated using per cycle static-stress SCC correlations.
415 However, the hold-time data analyzed here shows the time-dependent component is
416 accelerated by periodic fatigue stress cycles. Fig. 6 shows a comparison of predicted and
417 measured per cycle crack growth, da/dN, using the Wei-Landes superposition model.

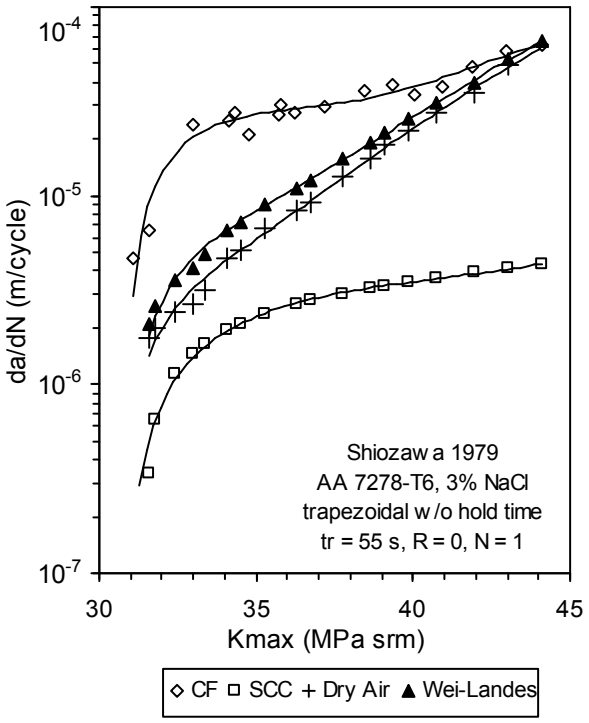

418

419 Fig. 6. Comparison of predicted and measured per-cycle crack growth using the Wei-Landes
420 superposition model. This figure shows that the Wei-Landes model (▲) significantly under predicts
421 the measured CF data (◊) for all but the largest $K_{\max}$ where $(da/dN)_{CF}$ and $(da/dN)_{inert}$ converge.

422

423 This figure shows that the Wei-Landes model significantly under-predicts the
424 measured CF data for all but the largest $K_{\max}$ where $(da/dN)_{CF}$ and $(da/dN)_{inert}$ (dry air)
425 converge. Then the data trends in Figs. 3(a), 3(b) and (6) are in contradiction to the Wei-
426 Landes model assumptions. Rather than a simple superstition of fatigue and SCC CGRs, the
427 analysis of the data presented here and elsewhere suggests that $\dot{a}_{env}$, within upper limits of

428 K_{max} and frequency, is due to a synergistic interaction of fatigue and SCC mechanisms (C-
429 SCC).

430 **6. Summary**

431 The purpose of this study is to consider how corrosion fatigue and stress-corrosion
432 cracking may act synergistically to produce environmental crack growth rates greater than
433 simple addition as assumed in superposition models. A phenomenological model was
434 developed to show that fatigue stress-cycles can synergistically accelerate SCC crack growth
435 rate (CGR) mechanisms by increasing the electrochemically-active surface area (ECSA) at a
436 crack tip. Activation of the crack tip is modeled as a competition between crack tip strain rate
437 (CTSR)-driven activation and corrosion-driven repassivation. The model was used to
438 calculate ECSA as a function of three CTSR components and activation-repassivation rate
439 constants. The model was fitted, with one adjustable parameter, to measurements of
440 environmental CGRs, which were reported as a function of stress intensity factor, fatigue
441 cycle rise-times and stress hold times.

442 **7. Conclusions**

443 1. Crack tip strain rate is an essential variable contributing to environmental cracking. In
444 order to model time-domain crack growth rates during (1) continuous cycling, (2) hold-
445 times and (3) static-load, crack tip strain rates must include strain rates due to (1)
446 variation in applied load, (2) strain rate due to crack advance, and (3) time-dependent
447 strain rate.

448 2. Strain rates due to fatigue stress-cycles increase the electrochemical activity at a
449 crack tip and thereby synergistically increase crack growth rates by the C-SCC
450 mechanism.

451 3. Crack tip strain rate activates crack tip surfaces well beyond that measured on a
452 strain-free bare metal surface, as is commonly used to measure repassivation rates for
453 stress corrosion models.

454 4. Repassivation during a hold-time following a fatigue cycle takes place in kilo-seconds
455 while repassivation of a strain-free bare metal electrode takes place in less than one
456 second.

5. Repassivation-time is increased during a fatigue-cycle hold-time as CTSR is sustained by continuing crack advance.
6. Synergism of fatigue stress-cycles and cyclic-stress corrosion-cracking produces environment-assisted cracking rates greater than those predicted by conventional superposition models.
7. Repassivation rate constants for use in SCC modeling should be obtained using straining electrodes instead of strain free electrodes currently in common use
8. A phenomenological model was developed to quantify the effects of fatigue stress-cycles on cyclic-stress corrosion-cracking crack-growth rates.

Declarations of Competing Interest: None

The author declares that there is no known competing financial interests or personal relationships that have influenced the work reported in this paper. This research did not receive any specific grant from funding agencies in the public, commercial, or not-for-profit sectors.

Data Sharing and Data Availability

Data sharing is not applicable to this article as no new data were either created or analyzed in this study. Data were “grabbed” from papers by Shiozawa (1979, 1984). Fitted model parameters are found in Table I and Table II.

References

[1][] Wei RP, Landes JD. Correlation between sustained-load and fatigue crack growth in high-strength steels. Mater. Res. Std. ASTM 9. 1969: 25-28.

[2][] Wei RP, Gao M. Reconsideration of the superposition model for environment assisted fatigue crack growth. Scr. Met. 1983; 17: 959-962.

[3][] Donahue JR, Lass AB, Burns JT. The interaction of corrosion fatigue and stress-corrosion cracking in a precipitation-hardened martensitic stainless steel. npj Mater. Deg. 2017; 1:11: 1-9. doi:10.1038/s41529-017-0013-2

[4][] Kovalovad D., Feketeb B., Engelhar GR, Macdonald DD. Prediction of corrosion fatigue crack growth rate in alloys. Part I: General corrosion fatigue model for aero-space aluminum alloys. Corros. Sci., 2018;141: 22-29.

[5][] Wei RP. Environmental considerations for fatigue cracking. Fatigue Fail. Eng. Mater. Str. 2002; 25: 845–854.

[6][] P.M. Scott, Environment-assisted cracking in austenitic components, Int. J. Pressure Vessels Piping 65 (1996) 255-264.

[7][] H.L. Craig, Jr., T.W. Crooker, D.W Hoeppner, Corrosion-Fatigue Technology, ASTM STP 642, American Society for Testing and Materials, (1976) 14-19.

[8][] W.Y. Maeng, Y.H. Kang, T.W. Nam, S. Ohashi, T. Ishihara, Synergistic interaction of fatigue and stress corrosion on the corrosion fatigue crack growth behavior in Alloy 600 in high temperature and high-pressure water, J. Nuc. Mat. 275 (1999) 194-200.

[9][] Toribio J, Kharin V. The reliability of the fracture mechanics approach to environmentally assisted cracking: 1. Uniqueness of the v(K)-curve. J. Mater. Des.1997;18: 87-94.

[10][] Somerday BP, Young LM, Gangloff RP. Crack tip mechanics effects on environment-assisted cracking of beta-titanium alloys in aqueous NaCl. Fatigue Fract. Engng. Mater. Struct. 2000; 23: 39-58.

[11][] Menana F, Hénaffb G. Synergistic action of fatigue and corrosion during crack growth in the 2024 aluminium alloy. Procedia Engineering 2010; 2: 1441–1450

[12][] Maenga WY, Kanga YH., Namb TW, Ohashic S, Ishiharad T. Synergistic interaction of fatigue and stress corrosion on the corrosion fatigue crack growth behavior in Alloy 600 in high temperature and high-pressure water. J. Nuc. Mater. 1999; 275: 194-200. https://doi.org/10.1016/S0022-3115(99)00114-2

[13][] Taylor CD. Review Article: Atomistic modeling of corrosion events at the interface between a metal and its environment. Inter. J. Corros. 2012; Hindawi Publishing Corporation Article ID 204640, 13 pages. doi:10.1155/2012/204640

[14][] Hosseini ZS, Dadfarnia M, Somerday BP, Sofronis P, Ritchie RO. On the theoretical modeling of fatigue crack growth. J. Mech. Phys. Solids, published online, Aug. 2018; doi: 10.1016/j.jmps.2018.07.026.

[15][] Turnbull A. Modeling of Chemistry and Electrochemistry in Cracks-A Review. Corrosion 2001; 57: 175-186.

[16][] Raicheff R. An electrochemical model for environmental cracking of metals. In: Gonis A., Turchi PEA., Kudrnovský J., eds. Stability of Materials. NATO ASI Series (B: Physics). 1996; 355: 669-676. https://doi.org/10.1007/978-1-4613-0385-5_51.

[17][] Hall Jr. MM. Critique of the Ford-Andresen film rupture model for aqueous stress corrosion cracking. Corros. Sci. 2009; 51: 1103-1106. DOI: 10.1016/j.corsci.2009.02.022

[18][] Hall Jr. MM. An alternative to the Shoji crack tip strain rate equation. Corros. Sci. 2008; 50: 2902-2905.

[19][] Hall Jr. MM. Effect of cyclic crack opening displacement rate on corrosion fatigue crack velocity and fracture mode transitions for Al–Zn–Mg–Cu alloys. Corros. Sci. 2014; 81: 132–143

[20][] Endo Konai K, Matsuda Y. Influence of stress ratios on cyclic stress corrosion crack growth characteristic of a high-strength steel. Bulletin of the JSME 1982; 24: 1885-1892.

[21][] Shiozawa K. Cyclic stress corrosion cracking of aluminum alloy. J. Soc. Mater. Sci. Japan 1979; 28: 92-98.

[22][] Shiozawa, K. Crack growth during cyclic stress corrosion cracking in aluminum alloy. J. Soc. Mater. Sci. Japan 1984; 33: 66-72.

[23][] Yokobori T, Yokobori, Jr. AT, Takasiu N. Stress hold-time, stress rate and frequency effects on fracture under corrosive environment and under high temperature creep, fatigue and creep-fatigue interaction conditions. In: Carlsson J. and Olhsen N.G. eds. Mechanical Behavior of Materials, Proc. 4th-Int. Conf. (ICM-4), Pergamon Press, Oxford 1983; 2: 967-981.

[24][] Henaff G, Menan F, Odemer G. Influence of corrosion and creep on intergranular fatigue crack path in 2XXX aluminum alloys. Eng. Fract. Mech. 2010; 77: 1975-1988.

[25][] Vermilyea DA. A theory for the propagation of stress corrosion cracks in metals. J. Electrochem. Soc. 1972; 119: 405-407.

[26][] Vermilyea DA. Concerning strain-enhanced corrosion mechanisms of SCC. Corrosion 1976; 32: 26-29.

[27][] Hall Jr. MM, Environmental Crack Driving Force. Metall. Mater. Trans. A 2013: 1200-1208. DOI https://doi.org/10.1007/s11661-012-1439-3.

[28][] Ford FP, Andresen PL. Environmentally assisted cracking in light water reactors, corrosion mechanisms. In: Marcus P, Ouder J, eds. Corrosion in Nuclear Systems. 1994: 501-546.

[29][] Sridha N, Brossia CS, Dunn DS, Anderko A. Predicting localized corrosion in seawater. Corrosion 2004; 60: 915-936.

[30][] McCrum IT, Janik MJ, Deconvoluting cyclic voltammograms to accurately calculate Pt electrochemically-active surface area. J. Phys. Chem. C. 2017; 121: 6237–6245, https://doi.org/10.1021/acs.jpcc.7b01617

[31][] Garrick TR, Moylan TE, Carpenter MK, Kongkananda A. Electrochemically active surface area measurement of aged Pt alloy catalysts in PEM fuel cells by co stripping. J. Electrochem. Soc. 2017; 164: F55-F59.

[32][] Polyanskii VM, N.I. Volkov NI, Gorodkova OM, Kopanov YuN, Frol'tsova TA, Khailov AN. Creep of medium and high strength aluminum alloys at normal temperature in moist atmospheres. Strength Mater. 1990; 22: 59-70, Translated from Problemy Prochnosti, 1990; No. I: 50-58.

[33][] Hui CY. The mechanics of self-similar crack growth in an elastic power-law creeping material. Int. J. Solids Structures 1986; 22: 357-372.

[34][] Hall Jr. MM. An alternative to the Shoji crack tip strain rate equation. Corros. Sci. 2008; 50: 2902–2905.

[35][]. Crack tip strain rate equation with applications to crack tip embrittlement and active path dissolution models of stress corrosion cracking. In: Environment-Induced Cracking of Materials, Volume 1, Chemistry, Mechanics and Mechanisms, Shipilov SA, Jones RH, Olive JM, Reback RB, eds. Elsevier, Oxford, UK. 2008: 59-68.

[36] Hall Jr. MM. Film rupture model for aqueous stress corrosion cracking under constant and variable stress intensity factor. Corros. Sci. 2009; 51: 225–233.

[37] Barsom JM. Effects of cyclic stress form on corrosion fatigue crack propagation below KI_{scc} in a high strength steel. In: Corrosion Fatigue: Chemistry, Mechanics and Microstructure, NACE-2, National Association of Corrosion Engineers 1972: 424–33.

[38] Huang Y, Nakajima A, Nishikata A, Tsuru T. Effect of mechanical deformation on permeation of hydrogen in iron. ISIJ International 2003; 43: 548-554.

[39] Larkin FS. Homogeneous rate of recombination of hydrogen atoms. Can. J. Chem. 1986; 46: 1005-1015.

[40] Raetzer-Scheibe HJ, Tuck CDS. The polarisation and repassivation behaviour of the aluminium-zinc-magnesium-copper Alloy 7010. Corros. Sci. 1994;36: 941-956.

[41] Cooper KR, Kelly RG, Crack tip chemistry and electrochemistry of environmental cracks in AA 7050. Corros. Sci. 2007; 49: 2636-2662.

[42] Atkinson KE. An Introduction to Numerical Analysis (2nd ed.). New York: John Wiley & Sons; 1986. ISBN 978-0-471-50023-0.

[43] Holroyd NJH, Hardie D. Strain-rate effects in the environmentally assisted fracture of a commercial high-strength aluminum alloy. Corros. Sci. 1983; 21: 129-144.

[44] Hall Jr. MM. Effect of cyclic frequency on fracture mode transitions during corrosion fatigue cracking of an Al-Zn-Mg-Cu alloy. Corros. Rev. 2015; 33: 315-334.

[45] Maeng WY, Kang YH, Nam TW, Ohashi S, Ishihara T. Synergistic interaction of fatigue and stress corrosion on the corrosion fatigue crack growth behavior in Alloy 600 in high temperature and high-pressure water. J. Nuc. Mat. 1999; 275: 194-200.

[46] Maa P, Liua C, Chenb Q, Wanga Q, Zhana L, Li J. Natural-ageing-enhanced precipitation near grain boundaries in high-strength aluminum alloy. J. Mater. Sci. Technol. 2020; 46:107-113.

[47] Harrison TJ, Crawford BR, Janardhana M, Clark G. Differing microstructural properties of 7075-T6 sheet and 7075- T651 extruded aluminium alloy. Procedia Engineering 2011; 10: 3117–3121.